Table XVII. Dipole Moments of Alkylphosphines

compd	exptl value[a]	MM3 value	difference	% difference
methylphosphine[b]	1.100 ± 0.010	1.184	0.084	7.64
dimethylphosphine[c]	1.23 ± 0.01	1.247	0.017	1.38
trimethylphosphine[d]	1.192 ± 0.005	1.173	-0.019	-1.59
trans-ethylphosphine[e]	1.226 ± 0.005	1.184	-0.042	-3.43
gauche-ethylphosphine[e]	1.22 ± 0.07	1.186	-0.034	-2.79
gauche-isopropylphosphine[f]	1.23 ± 0.01	1.186	-0.004	-3.58
tert-butylphosphine[g]	1.17 ± 0.02	1.196	0.026	2.22

[a] All values are in D. [b] Data from ref 14. [c] Data from ref 25c. [d] Data from ref 34. [e] Data from ref 36. [f] Data from ref 25i. [g] Data from ref 25h.

The fits to the experimental moments of inertia are reasonable, with the exception of *trans*-ethylphosphine. This error can be attributed to the fact that the geometry is calculated poorly for this conformer. The average deviation for the entire set of compounds is 1.10%. If the data for *trans*-ethylphosphine is discounted the average error is reduced by almost half to 0.62%. This is within the acceptable limit that can be accounted for from the systematic differences induced by MM3 calculating values based on r_g and microwave spectra giving r_a values.

Dipole Moments. Dipole moments have been determined for a number of the compounds under investigation in this study, either by microwave spectroscopy, ab initio calculations, or both. The comparison of the experimental and calculated dipole moments is presented as Table XVII. The calculated and experimental dipole moments for the molecules where data are available agree quite well. All values agree to within 0.1 D.

Conclusions

An MM3 force field has been developed that can model the structures, vibrational spectra, moments of inertia, and dipole moments of alkylphosphines with reasonable accuracy. These parameters represent a starting point for the development of MM3 parameters for other, biologically important, phosphorus-containing moieties, including phosphates and nucleotides. The incorporation of a torsion-bend parameter in future versions of molecular mechanics would allow for a more accurate representation of the conformers of ethylphosphine. This more accurate structural modeling would also increase the accuracy of the calculations of the moments of inertia, as well as the dipole moments and the barriers to rotation of these compounds.

Acknowledgment. This work was supported in part by grants from Burroughs Wellcome Inc., and Sterling Research.

Registry No. Phosphine, 7803-51-2; methylphosphine, 593-54-4; dimethylphosphine, 676-59-5; trimethylphosphine, 594-09-2; ethylphosphine, 593-68-0; isopropylphosphine, 4538-29-8; ethyldimethylphosphine, 1605-51-2; *tert*-butylphosphine, 2501-94-2.

Supplementary Material Available: Tables containing the comparisons between experimental and calculated vibrational assignments of *trans*- and *gauche*-ethylphosphine, *trans*- and *gauche*-isopropylphosphine, *trans*- and *gauche*-ethyldimethylphosphine, and *tert*-butylphosphine (13 pages). Ordering information is given on any current masthead page.

Probing Redox-Induced Molecular Transformations by Atomic-Resolution Scanning Tunneling Microscopy: Iodide Adsorption and Electrooxidation on Au(111) in Aqueous Solution

Xiaoping Gao and Michael J. Weaver*

Contribution from the Department of Chemistry, Purdue University, West Lafayette, Indiana 47907. *Received February 20, 1992. Revised Manuscript Received July 10, 1992*

Abstract: In-situ atomic-resolution scanning tunneling microscopy (STM) has been utilized on ordered Au(111) under electrode potential control in acidic aqueous solution to examine potential-dependent iodine adlayer structures formed by iodide electrooxidation as well as covalent electrosorption. In the potential region -0.3 to +0.4 V vs SCE, below where electrooxidation of solution iodide occurs, several distinct iodine adlayer structures were observed. At the most negative potentials, structures close to the hexagonal $(\sqrt{3} \times \sqrt{3})R30°$ ($\theta_I = 0.33$) pattern are evident. The registry between the adlayer and the substrate lattice was deduced in part from composite-domain images created by stepping the electrode potential so as to alter markedly the adsorbate coverage during acquisition of a given STM image. At potentials between -0.2 and +0.2 V, adlayer patterns progressively closer to the $(5 \times \sqrt{3})$ ($\theta_I = 0.4$) structure became increasingly prevalent. This features a diminution in the iodine spacing along two of the three iodine rows, with a corresponding ca. 5° shift from the $R30°$ direction. Above 0.2 V, the STM images indicate that predominant presence of more complex higher-coverage adlayers ($\theta_I \approx 0.44$) featuring long-range (19-22 Å) z corrugations rotated by 8-10° from the hexagonal iodine adlattice. These corrugations arise from periodic alterations in the iodine-binding site, necessitated by I-I distances that approach the van der Waals diameter. Above 0.3 V, however, polyiodide chains were also observed, featuring shorter (2.8-3.2 Å) I-I distances compatible with adsorbate-adsorbate chemical bonding; these increasingly distort the monomeric iodine superlattice structure. At the onset of solution iodide electrooxidation, at 0.45 V, *multilayer* iodine films were observed to form, consisting of polyiodide strands growing outward from a $(5 \times \sqrt{3})$ surface template. This STM spatial information is compared with structural data obtained previously from potential-dependent surface Raman spectra. The prospects of utilizing in-situ electrochemical STM to explore redox-induced surface molecular transformations are noted in the light of these findings.

The evolution of molecular-level structural techniques applicable directly to solid-liquid interfaces is having an increasingly profound impact on our fundamental understanding of electrochemical surface science.[1] Besides spectroscopic and diffraction methods,

0002-7863/92/1514-8544$03.00/0

scanning tunneling microscopy (STM) is emerging as an important new in-situ technique for this purpose. While most electrochemical applications of STM have so far been concerned with larger-scale surface morphology, a small yet growing number of recent reports demonstrate that the technique is capable of yielding *true* atomic resolution (i.e., spatial detection of individual surface atoms) at ordered metal–solution interfaces.[2-8] These include examples of molecular[4,6] and atomic adsorbates[2,3,5,8] as well as images of the metal substrate atoms themselves.[5,7]

In addition to discerning real-space structures for adsorbates under equilibrium conditions, it would be of considerable interest to utilize such in-situ atomic-resolution STM to deduce structural information for surface species involved in (or produced by) molecular transformations triggered by faradaic (i.e., redox) electrochemistry. The significance of such a quest is heightened by the wide variety of chemical transformations that can be induced to occur in a uniquely controllable fashion by electrochemical means. This approach might be expected to yield insight into the intramolecular adsorbate structure (bond distances, angles) as well as the superstructure of ordered adlattices formed by adsorbate arrays. As such, the real-space structural data furnished by STM should constitute an excellent complement to the adsorbate-bonding information provided in particular by in-situ vibrational spectroscopies.

We described here an example of this new tactic, specifically to the covalent adsorption of iodide and its electrooxidation to polyiodine species on ordered Au(111) in aqueous 0.1 M $HClO_4$. The Au(111) surface provides an interesting hexagonally ordered template for the reaction; we have recently described detailed in-situ STM on this face[5b] as part of a broader examination of ordered gold surfaces.[5] The reaction was selected partly in view of our earlier surface-enhanced Raman (SER) study of iodide electrooxidation on polycrystalline gold which indicates that both polyiodides and iodine species are formed in a distinctly potential-selective fashion.[9] The present findings enable the real-space surface structures associated with both these stages of oxidation to be discerned in detail and the modes of initiation and growth of the iodine multilayers to be assessed. Together with a related study concerned with sulfide electrooxidation to polysulfur,[6] the results herein illustrate the substantial, yet so far essentially untapped, potential of in-situ STM for exploring reactive as well as adsorptive molecular electrochemistry.

Experimental Section

Most experimental details of the in-situ electrochemical STM procedures have been described elsewhere.[3,5,10,11] The microscope is a commercial Nanoscope II (Digital Instruments) with a bipotentiostat for electrochemical STM. The STM tips were 0.01-in. tungsten wire etched electrochemically in 1 M KOH and insulated with clear nail polish (wet 'n Wild, Pavion, Ltd.) so to minimize the occurrence of faradaic electrochemistry on the wire. All STM images were obtained in the so-called "height mode" (i.e., at constant current) and are unfiltered unless noted otherwise. The set-point current was typically 5–20 nA, and the bias voltage 10–300 mV (vide infra). The STM electrochemical cell walls were machined from Kel-F, with the substrate electrode surface forming the base.[11] Platinum wires were employed for the counter electrode and as a quasi-reference electrode. All potentials quoted here are versus the saturated calomel electrode (SCE); the stability of the quasi-reference electrode with respect to the SCE was checked in separate experiments in a conventional electrochemical cell.

The Au(111) crystal (hemisphere, 7-mm diameter) was grown, cut, and polished at Laboratoire d'Electrochimie Interfaciale CNRS, Meudon, France, by Dr. A. Hamelin; the nominal orientation is within ±0.25°. The crystal was flame-annealed immediately before each experiment, cooled in ultrapure water, and transferred to the STM cell protected by a drop of water.

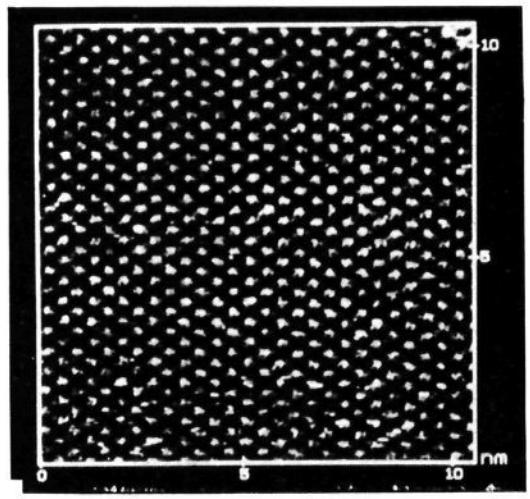

Figure 1. Unfiltered STM image of Au(111) in 0.1 M $HClO_4$ + 0.5 mM KI at −0.3 V vs *SCE*, showing approximate ($\sqrt{3} \times \sqrt{3}$) iodide adlayer. Imaging conditions: bias voltage V_b = 60 mV, set-point current i_t = 12 nA.

Results and Discussion

Equilibrium Iodide Adsorption. As a prelude to examining iodide electrooxidation, it is appropriate to discuss the interfacial structures for adsorbed iodide as deduced by STM at potentials below the value where solution-phase faradaic electrochemistry commences in 0.1 M $HClO_4$, ca. 0.4 V vs SCE. Most experiments utilized 0.5 mM iodide, although the concentration was varied over the range 0.01–20 mM with comparable surface-structural results. Figure 1 shows a representative unfiltered STM image obtained at −0.3 V vs SCE. The sharp spots can be deduced to constitute an ordered hexagonal layer exhibiting roughly ($\sqrt{3} \times \sqrt{3}$)*R*30° symmetry with respect to the underlying Au(111) lattice. Thus the spots lie 5.0 (± 0.3) Å apart (i.e., $\sqrt{3}$ times the gold atomic diameter, 2.88 Å), in directions approximately midway between [i.e., rotated 30 (±3)° from] the row orientations observed in the STM images for unmodified Au(111). The latter images could readily be obtained for the freshly annealed Au(111) in aqueous 0.1 M $HClO_4$ at potentials $\gtrsim$ 0 V vs SCE prior to iodide addition (see Figure 1 of ref 5b). [Some mild distortion of the simple (1 × 1) hexagonal array on Au(111), caused by a ($\sqrt{3}$ × 22) reconstruction, can be observed at negative electrode potentials.[5b] However, this reconstruction is lifted entirely by even low iodide coverages.] The observed near-($\sqrt{3} \times \sqrt{3}$) pattern arises unassailably from the surface binding of monomeric iodide. (As noted below, however, adsorbate-surface charge transfer occurs to yield essentially uncharged iodine atoms.)

Similar STM images of the apparently ($\sqrt{3} \times \sqrt{3}$)*R*30° structure (coverage = 0.33) on Au(111) have been reported recently in air for surfaces transferred from an iodide dosing solution[12a] and in water containing 10 mM NaI.[12b] We also have obtained similar images under ex-situ conditions. The present

(1) For example: Compton, R. G., Hamnett, A., Eds. *Comprehensive Chemical Kinetics*; Elsevier: Amsterdam, The Netherlands, 1989; Vol. 29.
(2) Magnussen, O. M.; Hotlos, J.; Nichols, R. J.; Kolb, D. M.; Behm, R. J. *Phys. Rev. Lett.* **1990**, *64*, 2929.
(3) (a) Yau, S.-L.; Vitus, C. M.; Schardt, B. C. *J. Am. Chem. Soc.* **1990**, *112*, 3677. (b) Schardt, B. C.; Yau, S. L.; Rinaldi, F. *Science* **1989**, *243*, 150.
(4) Yau, S.-L.; Gao, X.; Chang, S.-C.; Schardt, B. C.; Weaver, M. J. *J. Am. Chem. Soc.* **1991**, *113*, 6049.
(5) (a) Gao, X.; Hamelin, A.; Weaver, M. J. *Phys. Rev. Lett.* **1991**, *67*, 618. (b) Gao, X.; Hamelin, A.; Weaver, M. J. *J. Chem. Phys.* **1991**, *95*, 6993. (c) Gao, X.; Hamelin, A.; Weaver, M. J. *Phys. Rev. B* **1991**, *44*, 10983. (d) Gao, X.; Hamelin, A.; Weaver, M. J. *Phys. Rev. B*, in press.
(6) Gao, X.; Zhang, Y.; Weaver, M. J. *J. Phys. Chem.* **1992**, *96*, 4156.
(7) (a) Haiss, W.; Lackey, D.; Sass, J. K.; Besocke, K. H. *J. Chem. Phys.* **1991**, *95*, 2193. (b) Tao, N. J.; Lindsay, S. M. *Surf. Sci.* **1992**, *274*, L546.
(8) (a) Sachikata, K.; Furuya, N.; Itaya, K. *J. Electroanal. Chem. Interfacial Electrochem.* **1991**, *316*, 361. (b) Hachiya, T.; Honbo, H.; Itaya, K. *J. Electroanal. Chem. Interfacial Electrochem.* **1991**, *315*, 275.
(9) Tadayyoni, M. A.; Gao, P.; Weaver, M. J. *J. Electroanal. Chem. Interfacial Electrochem.* **1986**, *198*, 125.
(10) Chang, S.-C.; Yau, S.-L.; Schardt, B. C.; Weaver, M. J. *J. Phys. Chem.* **1991**, *95*, 4787.
(11) Vitus, C. M.; Chang, S.-C.; Schardt, B. C.; Weaver, M. J. *J. Phys. Chem.* **1991**, *95*, 7559.
(12) (a) McCarley, R. L.; Bard, A. J. *J. Phys. Chem.* **1991**, *95*, 9618. (b) Tao, N. J.; Lindsay, S. M. *J. Phys. Chem.* **1992**, *96*, 5213.

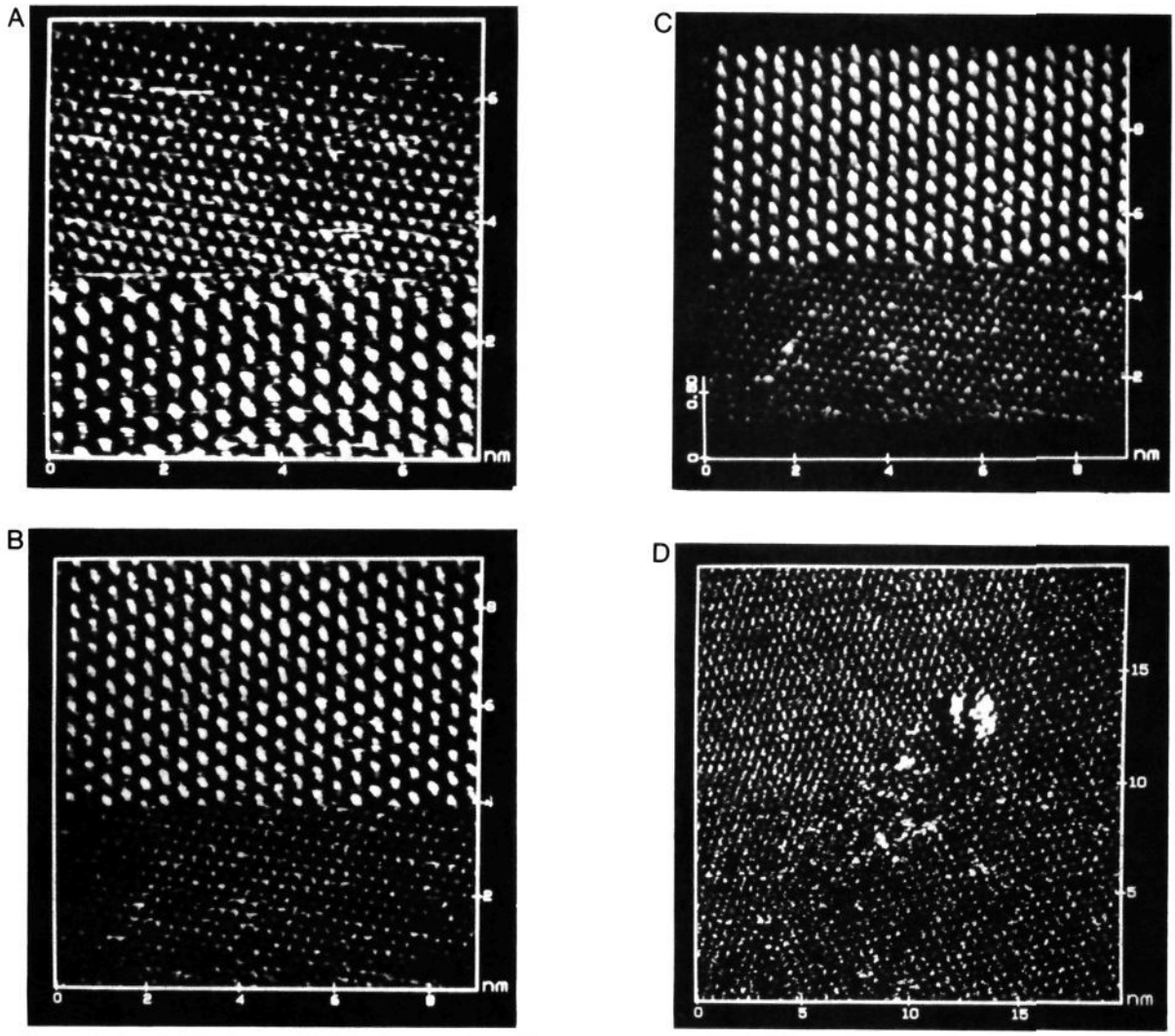

Figure 2. Composite-domain STM images of iodide adlayers on Au(111) in 0.1 M $HClO_4$ + 0.5 mM KI. (A) Bottom half is adlayer at −0.2 V having ca. (8 × √3) symmetry; top half is substrate image, obtained by stepping the potential to ca. −0.4 V during image acquisition. V_b = −15 mV, i_t = 20 nA. (B) Similar to A, but for iodide adlayer having (5 × √3) symmetry, formed by stepping the potential from −0.4 to 0.1 V during upward-rastered STM scan. (C) Filtered height-shaded view of B. (D) Obtained at 0 V, showing adjoining adlayer domains. V_b = −80 mV, i_t = 15 nA.

findings, however, constitute the first detailed results for this system under in-situ electrochemical conditions. A comparable (√3 × √3)*R*30° adlayer structure has been deduced recently for sulfide adsorption on Au(111) in 0.1 M $HClO_4$[6] and for alkanethiols on Au(111) in air.[13] In the former case, the sulfur binding was deduced to occur at 3-fold hollow sites on the basis of adjoining domain images containing the Au(111) substrate and adlattice patterns.[6]

Some other pieces of information, however, indicate that the registry between the iodine and Au(111) lattices tends to be somewhat less straightforward than described by the simple hexagonal (√3 × √3)*R*30° pattern. Parts A–D of Figure 2 show examples of STM images that are instructive in this regard. The first three (A–C) are "composite" images, obtained by stepping the potential roughly midway during the scan acquisition so to largely remove (or re-form) the iodine adlayer. Thus the bottom half of Figure 2A, showing an iodine adlayer image, was obtained at −0.2 V. As the tip scan (from right to left, rastered from top to bottom) reached midscreen, the electrode potential was stepped sufficiently negative (to ca. −0.4 V), so as to obtain a (1 × 1) Au(111) substrate image. The virtue of this tactic is that the registry between the iodine adlayer and the substrate can be obtained relatively accurately; the latter provides an internal calibration by which the deleterious effects of thermal drift in the STM image can be minimized.

By this means, the iodine adlayer can be seen to be distorted significantly (albeit slightly) from the hexagonal (√3 × √3) pattern, whereupon the interatomic distances along two of the three iodine rows are compressed by ca. 10% below the √3 distance (√3 × 2.884 Å = 5.0 Å) and shifted correspondingly (by ca. 3°) from the *R*30° direction. Parts B and C of Figure 2 show top-view and height-shaded images obtained similarly, by stepping from −0.4 to +0.1 V during the upward-rastered STM scan. These latter images show a comparable distortion of two of the three row directions, being compressed by ca. 15% and rotated by ca. 5° from the *R*30° substrate direction.

The iodine adlattice in Figure 2B,C provides a good fit to the (5 × √3) iodine symmetry ($\theta_I \simeq 0.4$) observed recently on Au(111) under similar conditions by means of low-energy electron diffraction (LEED) measurements following electrode emersion[14] and by high-precision STM in air.[15] This structure features a pair of iodine row directions shifted by 4.7° from the *R*30° direction, the atoms presumed to be located in binding sites which vary between 2-fold and 3-fold geometries. Perhaps surprisingly,

(13) Widrig, C. A.; Alves, C. A.; Porter, M. D. *J. Am. Chem. Soc.* **1991**, *113*, 2805.

(14) Bravo, B. G.; Michelhaugh, S. L.; Soriaga, M. P.; Villegas, I.; Suggs, D. W.; Stickney, J. L. *J. Phys. Chem.* **1991**, *95*, 5245.

(15) Haiss, W.; Sass, J. K.; Gao, X.; Weaver, M. J. *Surf. Sci.* **1992**, *274*, L593.

(16) Ocko, B. et al. To be published.

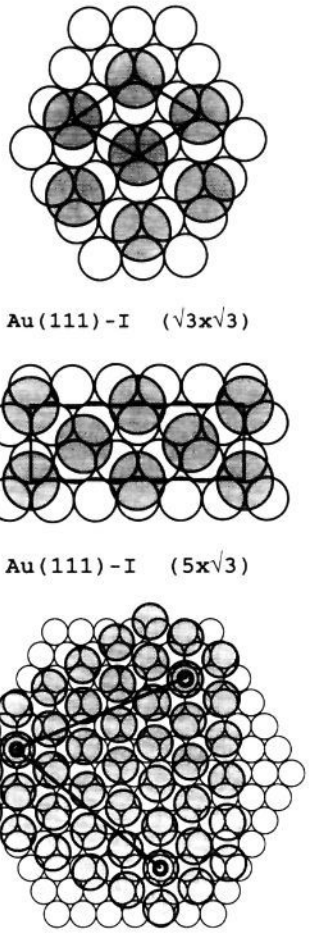

Figure 3. Ball models of the Au(111)–iodide layer structures discussed here. Gray-shaded circles depict iodine atoms; open circles are gold substrate atoms. Lines in parts A and B indicate the $(\sqrt{3} \times \sqrt{3})$ and $(5 \times \sqrt{3})$ unit cells, respectively. Lines in part C indicate half of the $(7 \times 7)R21.8°$ unit cell; the inner circles denote iodine atoms located at symmetric atop sites, corresponding to the brightest spots in the image in Figure 4.

however, no periodic z corrugations are evident in the STM images along the iodine rows; markedly more intense images (i.e., higher z displacements) have been observed for iodine atoms adsorbed at 2-fold bridging and especially atop sites compared with 3-fold hollow sites on Pt(111).[3,10]

As a consequence, the $(5 \times \sqrt{3})$ pattern can easily be mistaken for the lower-coverage $(\sqrt{3} \times \sqrt{3})$ structure, given the degree of x–y distortion commonly present in STM patterns as a result of thermal drift and other nonidealities. Similarly, as noted in ref 15, the LEED pattern for the former symmetry has been misidentified previously as the latter structure. A ball-model depiction of the $(5 \times \sqrt{3})$ structure is shown in comparison with the $(\sqrt{3} \times \sqrt{3})$ adlayer symmetry in Figure 3. (The gray-shaded circles represent iodine atoms, and the smaller open circles are the gold substrate atoms.) The suggested $(5 \times \sqrt{3})$ adlattice shown in Figure 3B features the corner iodines (in the unit cell as shown) sited in slightly asymmetric 3-fold sites. Such an arrangement results in each of the four iodines contained within the $(5 \times \sqrt{3})$ unit cell being situated in asymmetric sites between 2- and 3-fold geometries; this particular structure can rationalize the observed near-equivalence of each of the iodine atoms in the observed STM images.

On this basis, the iodine adlayer domain seen in Figure 2A is likely to have a structure intermediate between $(5 \times \sqrt{3})$ and $(\sqrt{3} \times \sqrt{3})$, which we can denote as approximately $(8 \times \sqrt{3})$. Interestingly, preliminary in-situ X-ray diffraction measurements of the Au(111)–I system indicate the presence of adlayer symmetries lying between these discrete distorted hexagonal structures, the iodine interatomic distances apparently compressing continuously as the iodine coverage increases toward higher electrode potentials. We have observed similarly continuous potential-induced alterations in adlayer symmetries for iodide on Au(100) and Au(110) by STM. Unlike the case of Au(111), periodic z corrugations are observed for these adlayers which assist the detection of such subtle structural changes. (These findings will be described elsewhere.) It would be of obvious interest to undertake an extremely detailed potential-dependent STM study on Au(111) to compare with such precise diffraction results for the present system. A relevant issue is whether uniform adlayer structures are formed at a given electrode potential or mixtures of domains having significantly different adlayer symmetries (and iodine coverages) are present instead. A clear answer to this question would require more precise (and abundant) STM data on the system than have been acquired so far. The image shown in Figure 2D nonetheless illustrates a commonly observed phenomenon of two rotated iodine adlayer domains within a given substrate terrace region. Careful inspection of this image in comparison with that for the corresponding substrate suggests that the domain lying toward the top left-hand corner has a structure, ca. $(8 \times \sqrt{3})$, closer to the symmetric $(\sqrt{3} \times \sqrt{3})$ pattern, whereas the remaining adlayer exhibits a packing close to $(5 \times \sqrt{3})$. Such iodine domain boundaries are observed to form even within a uniform *gold substrate* domain.

Distinctly different STM images are observed preferentially at potentials positive of 0.2 V vs SCE. A representative example is shown in Figure 4A,B. (The tip-substrate bias voltage for this image, −200 mV, is larger than that employed typically at lower electrode potentials in order to avoid complications from tip oxidation; similar results were obtained, however, using less negative bias voltages.) Several aspects of these images are noteworthy. First, while the rows of iodine atoms together form a near-hexagonal array, the d_{I-I} values are about 4.4–4.5 Å, significantly below the $\sqrt{3}$ distance of 5.0 Å. Second, longer-range z corrugations (i.e., variations in the "effective height") of the iodine atoms are clearly observed, forming a hexagonal pattern with a periodicity ranging from 19 to 22 Å. This superlattice is rotated (in either direction) from the iodine hexagonal lattice by about 8–10°. Similar structures were obtained on Au(111) in air using a high-precision "beetle-type" STM.[15] The data indicate that the $R30°$ substrate direction lies between the iodine rows and the z corrugations, being rotated from the former by about 4°. Careful examination of a number of images yields d_{I-I} values of 4.35 (±0.1) Å, corresponding to iodine coverages around 0.44, so that the adlayer structure approaches the close-packed limit ($\theta_I \approx 0.45$) determined by the iodine van der Waals diameter, 4.3 Å.[17] The potential-induced progression between the several adlayer arrangements described so far are reversible, the lower-coverage $(5 \times \sqrt{3})$ and the near-$(\sqrt{3} \times \sqrt{3})$ structures being recovered upon readjusting the electrode potential to appropriately lower values.

The form of the observed superlattice in Figure 4 is reminiscent of the "charge-density waves" observed by STM and diffraction methods at semiconductors and (to a smaller extent) on metal surfaces.[18] Indeed, the magnitude of the z corrugations can be attenuated markedly for small negative bias voltages, suggesting that such a periodic electronic effect may be present here. However, the present longer-range corrugations reflect at least in part periodic variations in the iodide surface binding sites necessitated by the noncommensurate nature of the close-packed iodine and gold substrate lattices. The regions of "tunneling maxima" (i.e., higher z values) are probably associated with iodide being bound in atop (or near-atop) binding sites rather than being nestled in 2-fold briging or especially 3-fold hollow sites as in the lower-coverage adlayers. [Again, clear-cut evidence for markedly more efficient electron tunneling via atop versus multifold iodine

(17) Gordon, A. J.; Ford, R. A. *The Chemist's Comparison*; Wiley: New York, 1972; p 109.

(18) For example: Lieber, C. M.; Wu, X. L. *Acc. Chem. Res.* **1991**, *24*, 170.

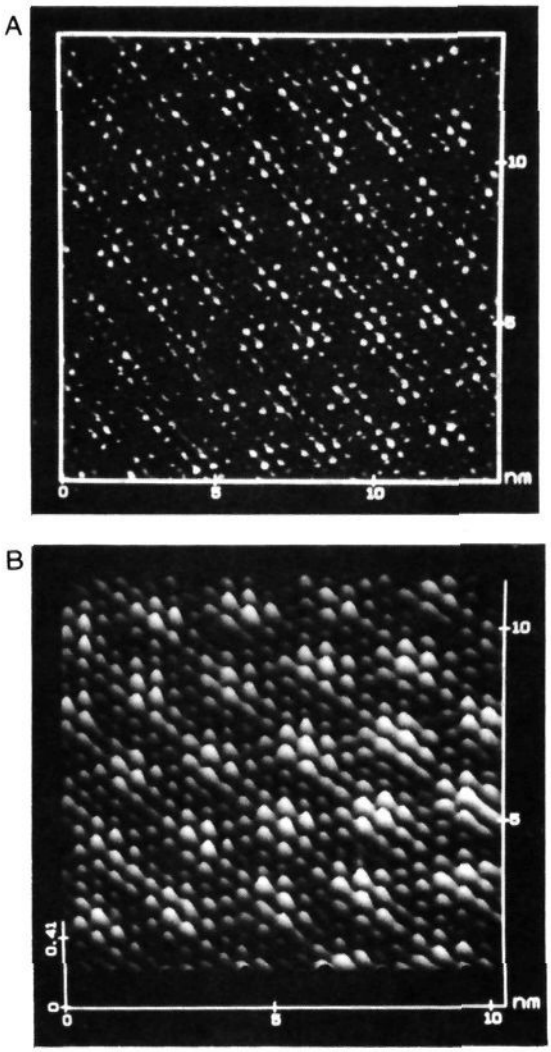

Figure 4. (A) Unfiltered top view and (B) filtered height-shaded STM image of "high-coverage superlattice" iodide adlayer, obtained as in Figures 1 and 2 but at 0.3 V. $V_b = -300$ mV, $i_t = 20$ nA.

has been obtained for the Pt(111)–I system.[10]] Structures yielding longer-range periodicities in the iodine binding sites in accord with the observed z corrugations can readily be constructed on the basis of the adlayer real-space parameters noted above. Such periodicities are not inconsistent with the LEED pattern observed for the saturated-coverage adlayer formed on Au(111) by gas-phase iodine dosing, featuring hexagonal fractional-order features.[19]

Figure 3C displays a suggested half-cell ball model for our high-coverage "incommensurate" structure, having the symmetry $(7 \times 7)R21.8°$, in comparison with the $(\sqrt{3} \times \sqrt{3})$ and $(5 \times \sqrt{3})$ adlayer unit cells shown in Figure 3A,B. The progressively higher coverages (0.33, 0.4, and ca. 0.45) associated with these structures, observed at increasing electrode potentials, are seen to be achieved by systematic decreases in the d_{I-I} values below the $\sqrt{3}$ value, 5.0 Å, together with rotation of two or more iodine rows with respect to the $(\sqrt{3} \times \sqrt{3})$ structure.

The potential-dependent iodine coverages determined by Auger spectroscopy after electrode emersion as reported by Bravo et al.[14] are approximately consistent with the adlayer structures observed in the present work; θ_I is seen to approach 0.45 by about 0.4 V vs SCE. Quantitative iodide coverage–potential data are also obtainable directly from sequences of electrode capacitance–potential data for various electrolyte compositions. The form of individual capacitance–potential curves for the Au(111)-aqueous iodide system indicates that near-saturation coverages are reached within the potential range studied here.[20]

Initial Iodide Electrooxidation. So far, we have considered adlayer structural features identifiable unambiguously as arising from iodide chemisorption in the *formal* absence of faradaic processes. It is nonetheless appropriate to recall that anion adsorption itself inevitably involves some charge transfer to the surface arising from bond covalency.[23] Indeed, iodide binding to gold appears to yield almost complete charge transfer on the basis of the adsorption thermodynamics ("electrosorption valency")[24,25] and X-ray photoelectron spectroscopy,[14] so that the adsorbate can be considered to be iodine adatoms rather than iodide ions. Regardless of the degree of such adsorbate charge transfer, however, the range of electrode potential over which iodide chemisorption occurs is not necessarily related to the potential at which the electrooxidation of *solution-phase* iodide commences. Under the present conditions, the latter process (yielding triiodide) is seen from voltammetric data to be initiated at a potential, E_{ox}, of about 0.45 V vs SCE.[9]

Nevertheless, it is of considerable interest to examine the effects of such solution faradaic processes upon the iodine adlayer structure. The significance of this question can be couched in thermodynamic terms: for $E \gtrsim E_{ox}$, zerovalent iodine becomes stable in the form of I_2 (and polyiodide species) as well as by binding to the gold substrate. As a consequence, one anticipates that iodine adlayer structures could be formed on gold in this potential region in the presence of solution iodide that are influenced, or even dominated, by I–I rather than by Au–I bonding. This expectation is heightened by our previous deduction by means of SER spectra that polyiodide species are formed on gold under the present conditions at potentials above ca. 0.2 V.[9]

Intriguingly, examination of STM images on Au(111) in the potential region 0.3 to 0.4 V vs SCE yields direct information on the structure of the polyiodide chains thus formed. Parts A–E of Figure 5 show examples of STM images taken under these conditions. The first three images (Figure 5A–C) illustrate the nature of the initially deposited polyiodide strings and their relation to the ordered iodine adlayer. Parts A and B of Figure 5 show the disruption, presumably disordering, caused in the corrugated iodine adlayer by chain growth. The initial stages of polyiodide formation also result in interesting alterations in the row directions of the underlying iodine adlayer, as evident in Figure 5C. While no one unique chain structure could be discerned, Parts C–E of Figure 5 show a common tendency of the iodine strings to form hexagonal-shaped arrays roughly 30 Å across. Unlike the ordered iodine adlayers, however, the strongs tend to lie *along* the direction of the gold substrate rows. As seen most clearly in Figure 5D, the iodine rows consist preferentially of three- to five-atom strings, with an interatomic spacing of 2.9 (±0.4) Å. In some cases, side-by-side pairs of rows were observed, again running parallel to the substrate atoms.

These features resemble the polyiodide structures commonly observed in bulk-phase crystalline environments.[26] The bond distances within the iodine strings, d_{I-I}, are comparable to those, 2.8–3.4 Å, found in polyiodides, although lacking the clear-cut

(19) Cochran, S. A.; Farrell, H. H. *Surf. Sci.* **1980**, *95*, 359.

(20) Thus capacitance–potential (C_d–E) curves obtained on Au(111) for higher iodide concentrations display a pair of maxima,[21] indicating the formation of intermediate coverages by ca. −0.5 V vs SCE; C_d reaches lower, potential-insensitive values for $E > -0.2$ V, suggesting an approach to surface saturation. (See ref 22 for explanations of the underlying thermodynamic analysis.) A comparison between coverage-potential information for iodide on ordered gold surfaces extracted from such C_d–E data and from STM measurements will be undertaken elsewhere.

(21) (a) Hamelin, A.; Bellier, J.-P. *Surf. Sci.* **1978**, *78*, 159. (b) Edens, G.; Hamelin, A. Unpublished observations.

(22) Hupp, J. T.; Larkin, D.; Weaver, M. J. *Surf. Sci.* **1983**, *125*, 429.

(23) For example: Schultze, J. W.; Koppitz, F. D. *Electrochim. Acta* **1976**, *21*, 327.

(24) Rath, D. L.; Hansen, W. N. *Surf. Sci.* **1984**, *136*, 195.

(25) Deakin, M. R.; Li, T. T.; Melroy, O. R. *J. Electroanal. Chem. Interfacial Electrochem.* **1988**, *243*, 343.

(26) For example: (a) Hon, P. K.; Mak, T. C. W.; Trotter, J. *Inorg. Chem.* **1979**, *18*, 2916. (b) Herbstein, F. H.; Schwotzer, W. *Angew. Chem., Int. Ed. Engl.* **1982**, *21*, 219. (c) Dubler, E.; Linowsky, L. *Helv. Chim. Acta.* **1978**, *58*, 2604.

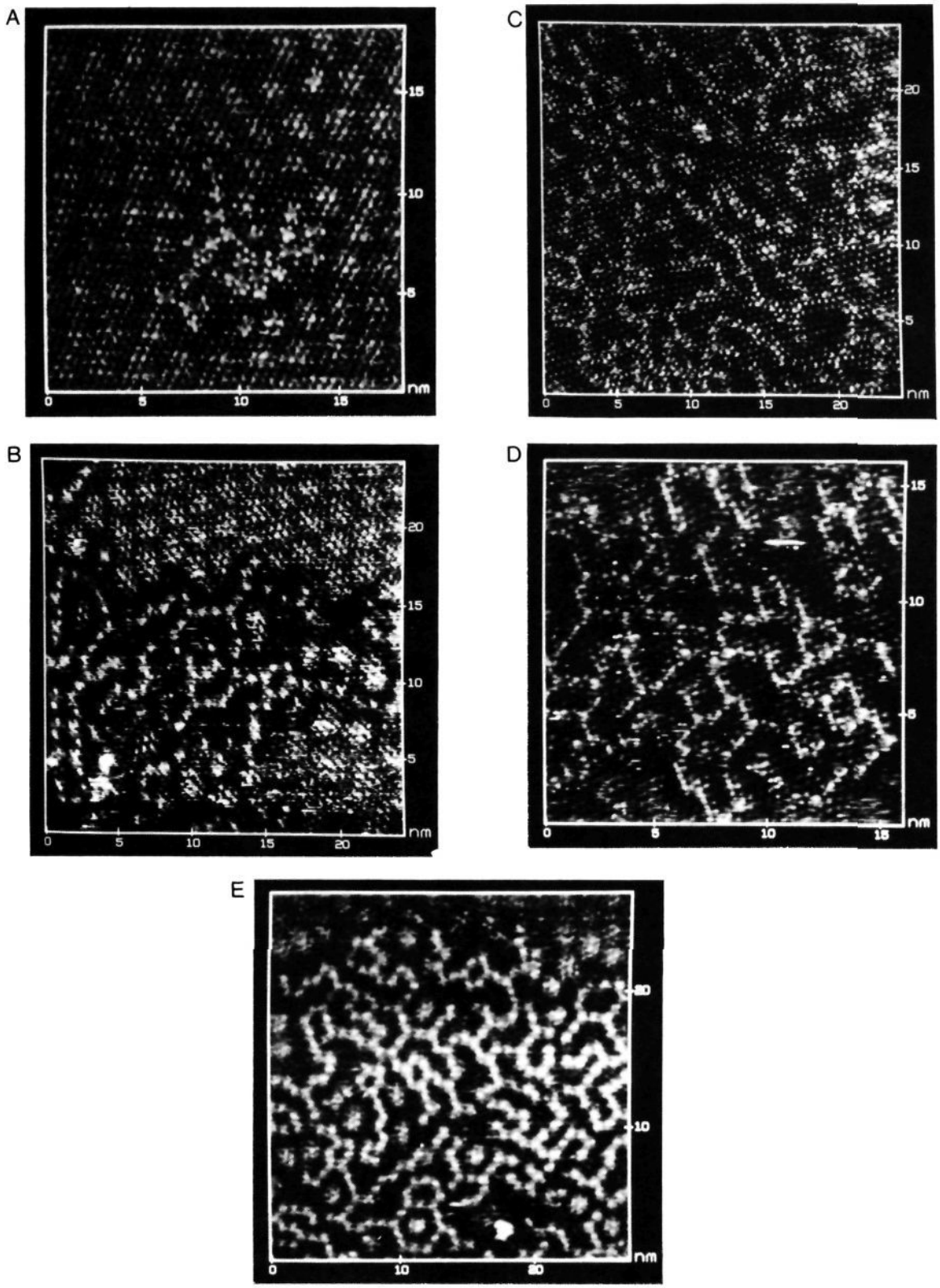

Figure 5. STM images showing formation of polyiodide chains on a superlattice adlayer, obtained as in Figures 1 and 2 but at 0.3–0.4 V. $V_b \simeq -200$ mV, $i_t \simeq 10$ nA.

alternation in d_{I-I} found for the latter. This suggests that the anionic charge in the surface polyiodide chains is delocalized, rather than being centered primarily on every alternate iodine atom. The role of the gold substrate in providing a template for the polyiodide strands is clearly evident not only from the observed row directions but also from the approximate equality between d_{I-I} and the gold interatomic spacing, 2.9 Å.

These spatial structural features offer an interesting comparison with the SER vibrational spectra for this system.[9] Besides the 123/158 cm^{-1} doublet due to the iodine adlayer, the formation of interfacial polyiodide is signaled by a band at 110 cm^{-1}, probably due to the I_3 symmetric stretch, along with an intense feature at 145 cm^{-1}, attributed tentatively to the "outer" vibrational mode of I_5.[9] It should be borne in mind that these SER spectra and

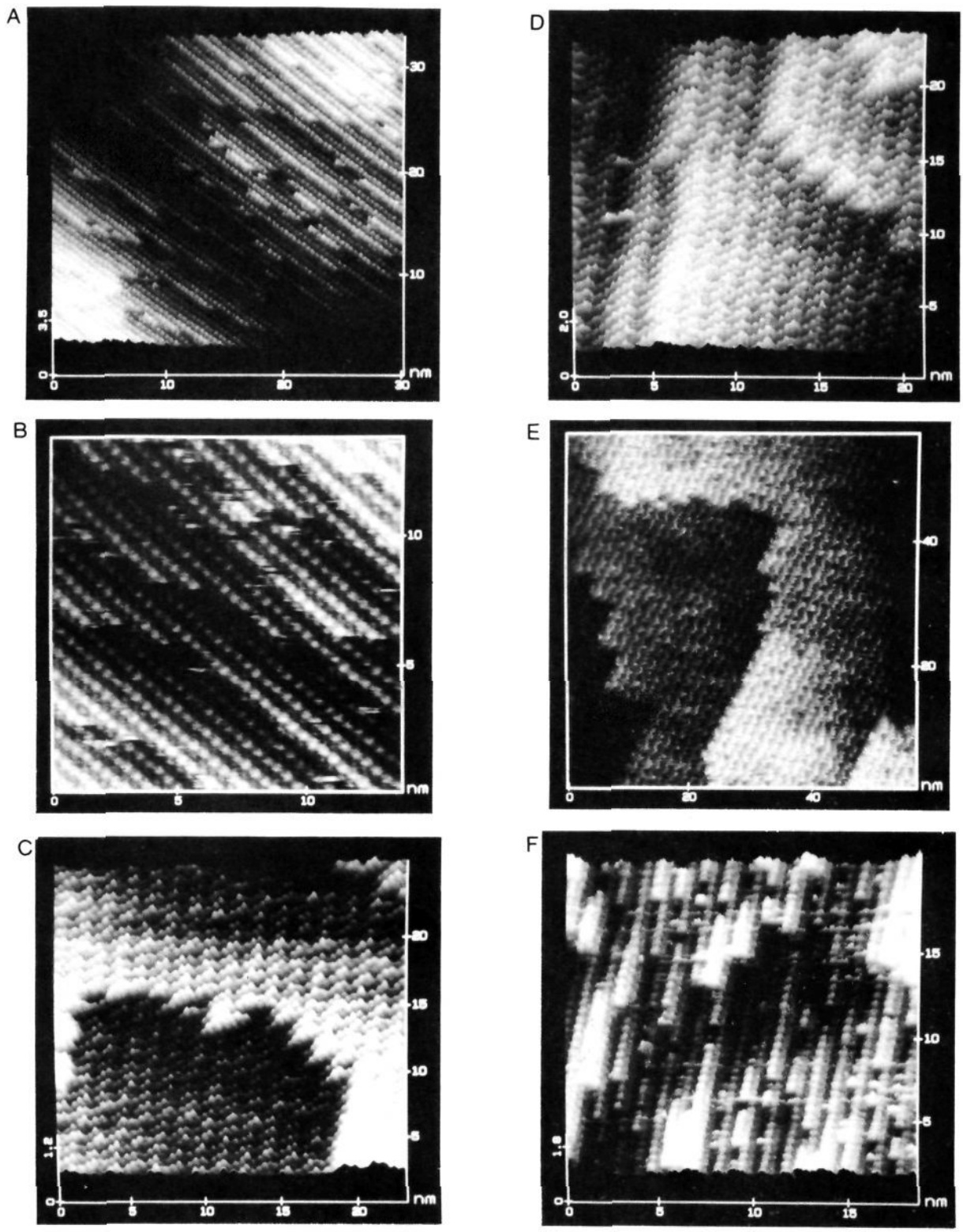

Figure 6. STM images showing formation of multilayer iodine films, obtained as in Figures 1 and 2 but at 0.4 V (A–E) after holding potential at 0.45 V for ca. 30 s (see text). Image F was obtained after returning potential to −0.1 V for 10 min. $V_b \simeq -200$ mV, $i_t \simeq 10$ nA (A–E); $V_b = 100$ mV, $i_t = 15$ nA (F).

accompanying STM structural features are observed at potentials, 0.2–0.4 V vs SCE, *below* where detectable steady-state anodic current to form *solution* polyiodide commences. Evidently, then, such interfacial polyiodide chains are stabilized significantly by surface interactions, consistent with the influence of the gold substrate on the chain structure as discerned by STM.

Iodine Film Formation. Increasing the potential up to values, ca. 0.45 V, where anodic current is clearly detectable, yields dramatic changes in the STM images. Parts A–D of Figure 6 are representative height-shaded images obtained at ca. 0.4 V after iodide electrooxidation has proceeded in this manner at 0.45 V for ca. 30 s. The tip-substrate bias voltage was again set usually to ca. −200 mV, in order to maintain the tip potential at values below where tungsten electrooxidation causes damage to the tip morphology. While a rich array of structural features arising from multilayer iodine films can be observed, the images contain some

persistent patterns. The parallel strings observed most clearly in Figure 6A lie along one of the $\sqrt{3}$ directions (i.e., $R30°$ to the gold substrate rows). The distance between parallel, equivalently imaged, rows in Figure 6A is 7.2 (0.5) Å, with an interatomic spacing along the rows of 5.0 (±0.4) Å. Interestingly, these lattice dimensions are commensurate with the $(5 \times \sqrt{3})$ unit cell for the adsorbed iodide discussed above (Figure 3B). Thus the unit cell as drawn features vertical iodine strings with interatomic distances of 5.0 Å along the rows. Adjacent rows alternate between essentially 3-fold and 2-fold iodine binding, the separation between every second (sterically equivalent) string being 7.2 Å. While the distance between most iodine rows in Figure 6A is 7.2 Å, "in-between" rows are also observed; these are more evident in the top-view image shown in Figure 6B.

Consequently, then, the iodine adlayers produced upon iodide electrooxidation have some structural features in common with at least one of the iodide adlattices present at lower potentials. Most probably, the $(5 \times \sqrt{3})$ ($\theta_I = 0.4$) adlayer provides a template for growth of *multilayer* iodine films. The presence of additional iodine layers (i.e., growing in the z direction) is clearly evident from the STM images. For example, segments of higher (i.e., brighter) iodine rows can be discerned, typically being ca. 2 Å higher than the adjoining strings.

Figure 6C shows a significantly different multilayer iodine pattern. Nonetheless, iodine strings are again present along a $\sqrt{3}$ direction, rotated 60° counterclockwise to the adlayers in Figure 6A,B. (Note that the substrate x–y orientation in Figure 6A–F is the same.) The interatomic spacings in Figure 6C are also as before, although some longer-range periodicities are now evident. An instructive feature of Figure 6C is the terrace edge sweeping through the middle of the image. The step height is about 4 Å. Rather than being a vertical step, however, it appears to be slanted by roughly 25° to the x–y plane. Within this step, four or five iodine atoms can be discerned.

Taken together, these details enable a structural model for the growing multilayer iodine film to be ascertained. Polyiodide (or polyiodine) strings are apparently propagated from each iodine atom in the $(5 \times \sqrt{3})$ template, so as to form a relatively close-packed multilayer film. The remarkable conducting properties of the film are evident from the observation of high-quality STM images even for films that are at least 5–10 iodine atoms thick. The iodine strings appear to be tilted, with their close-packed nature nonetheless yielding long-range order in the x–y plane. The propagation of the films in the z direction is driven by the formation of stable polyiodide chains; their continued growth is facilitated by the excellent electron transmission along the chain direction. Growth of the iodine film in the z direction is also very uniform, although the outer surface of the film can exhibit differing corrugated features. A clear example of the latter is evident in Figure 6D. This film is reminiscent of a "stepped" metal surface, with regular corrugations (steps) running close to the y direction. Another variant of a "stepped" iodine superstructure is shown in Figure 6E.

Adjusting the potential back to negative values following anodic film formation yields marked alterations in the STM image. Unlike the potential-dependent adlayers formed prior to iodide electrooxidation, however, some irreversibility is encountered in that the structural arrangements summarized in Figure 3 are not recovered entirely under these conditions. As an illustration, Figure 6F shows an atomic-resolution image obtained at −0.1 V following iodine film formation at 0.45 V. Sharply corrugated atomic strings are maintained along one $\sqrt{3}$ direction, with a 5-Å interatomic spacing. Apparently, then, segments of the anodically formed iodine film are still present even at potentials well below those corresponding to the reduction of solution iodine (or polyiodide). These features may well reflect some disruption of the gold substrate lattice attending iodine film formation.

Concluding Remarks

The foregoing results demonstrate some substantial virtues of in-situ STM with atomic resolution for elucidating detailed potential-dependent adlayer structures at ordered electrochemical interfaces. The registry between the adlattice and the substrate, and even the adsorbate binding sites, can be elucidated in favorable cases, as here, from STM images featuring adjoining adlayer and substrate domains. The present system offers an intriguing opportunity to explore not only the potential-induced evolution of discrete and distinct iodide adlayer structures but also their relation to the polyiodide/iodine layers that are formed anodically at higher potentials. Three chemically distinct interfacial states of essentially zerovalent iodine, formed in a potential-selective fashion, can be delineated from the STM data. First, the adlayers formed below the iodide oxidation potential involve monomeric iodine, stabilized solely by surface-adsorbate bonding. The second state involves polyiodide strings propagating along the surface, and stabilized by Au–I as well as I–I bonding, so as to form significantly below the oxidation potential of solution iodide, E_{ox}. Third, multilayer iodine/polyiodide films are formed when $E \gtrsim E_{ox}$ that, while obviously stabilized primarily by I–I bonding, are seen to grow from a $(5 \times \sqrt{3})$ surface template. The central role of the Au(111) substrate symmetry in controlling the adlayer structures at all three of these stages is therefore clearly evident.

The utilization of in-situ atomic-resolution STM to explore such redox-induced interfacial chemistry would appear to be applicable to a wide range of reactive adsorbates, even though there are inevitable limitations, such as the need for an immobile adlayer for satisfactory imaging. Most importantly, the technique enables the unique control of redox chemical events provided by electrochemical systems to be harnessed for the exploration of surface molecular transformations in an extremely flexible as well as detailed fashion. Recent examinations of underpotential deposited metal adlayers by means of in-situ STM provide a related example of this tactic.[3,8] Such applications of STM clearly have much to offer surface chemistry in general, as well as electrochemistry in particular.

Acknowledgment. We are grateful to Dr. Antoinette Hamelin for preparing the Au(111) crystal used here. We also thank Dr. Ben Ocko for sharing some of his X-ray diffraction data prior to publication.[16] This work is supported by the Office of Naval Research and the National Science Foundation.

Registry No. Au, 7440-57-5; I^-, 20461-54-5; I_2, 7553-56-2.